Controllable Perovskite Crystallization by Water Additive for High-Performance Solar Cells

Xiu Gong, Meng Li, Xiao-Bo Shi, Heng Ma, Zhao-Kui Wang, and Liang-Sheng Liao**

A key issue for perovskite solar cells is the stability of perovskite materials due to moisture effects under ambient conditions, although their efficiency is improved constantly. Herein, an improved $CH_3NH_3PbI_{3-x}Cl_x$ perovskite quality is demonstrated with good crystallization and stability by using water as an additive during crystal perovskite growth. Incorporating suitable water additives in *N*,*N*-dimethylformamide (DMF) leads to controllable growth of perovskites due to the lower boiling point and the higher vapor pressure of water compared with DMF. In addition, $CH_3NH_3PbI_{3-x}Cl_x \cdot nH_2O$ hydrated perovskites, which can be resistant to the corrosion by water molecules to some extent, are assumed to be generated during the annealing process. Accordingly, water additive based perovskite solar cells present a high power conversion efficiency of 16.06% and improved cell stability under ambient conditions compared with the references. The findings in this work provide a route to control the growth of crystal perovskites and a clue to improve the stability of organic–inorganic halide perovskites.

1. Introduction

Organic–inorganic halide perovskite solar cells (PSCs) have attracted significant attentions in recent years owing to their many advantages such as broad and strong light absorption,[1] long charge carrier diffusion length,[2,3] bipolar transport properties,[4,5]and longer carrier lifetimes.[6,7] The power conversion efficiency (PCE) have reached a high efficiency of 20.1%[8,9] within a few years from initial 3.81%[10] reported in 2009. Initially, one-step precursor deposition method to form perovskite films and mesoporous structure based PSCs was mostly reported. However, the morphology of perovskite films is hard to control. Subsequently, TiO_2 or Al_2O_3 scaffolds based PSCs were demonstrated with PCE over 15%.[11,12] Recently, planar structure based PSCs have been proposed because of their simple device architecture, easy fabrication procedure, and low temperature processing. Many innovative approaches have been used to improve the performance of planar PSCs, such as PCE in 15.4% by dual-source vapor deposition technique,[5] 13.9% by a solvent-induced fast crystallization,[13] 13.1% by alkyl halide additives,[14] 15.1% by poly(3,4-ethylene-dioxythiophene):polystyrenesulfonate (PEDOT:PSS)-GeO_2 underlayer modification,[15] 15.7% by cathode and anode dual modifications.[16]

Despite the device efficiency has achieved significant progress, these perovskite solar cells have to be fabricated in very rigorous condition, i.e., in glove box with a humidity less than 1%.[17,18] To enable PSCs' commercial applications, one large challenge is to resolve the cell stability issue because the perovskite films would be degraded gradually with time in air.[12,19] To date, a few studies have been focused on the processing circumstance and the stability issue of perovskite solar cells. You et al.[20] investigated the effect of humid environment on the thermal annealing of perovskite precursor films. Bass et al.[21] reported that the moisture can prompt the crystallization of lead organohalide perovskites into the expected cubic phase. Yang et al.[22] demonstrated a flexible PSC with a PCE of 7.14% which was fabricated under ambient. These studies suggest that the moisture plays an important role in the performance of perovskite solar cells. However, few studies focus on the mechanism how the moisture affects the cell degradation. In addition, controllable growth of the crystalline perovskite films is regarded as the most important factor to obtain high-efficiency PSCs. In general, the growth of crystalline perovskite films is sensitively dependent on the solution concentration, precursor composition, solvent choice, deposition temperature, and so on. Crystallization controlling by manipulating the perovskite nucleation and growth can improve the film morphology and coverage effectively.[22,23] Especially, solvent engineering plays very fascinating role in the controllable growth of solution-processed crystalline films. Liang et al. reported that crystallization rate of perovskites could be controlled by incorporating 1,8-diiodooctane (DIO) additives into the precursor solution.[24] Song et al. demonstrated that perovskite crystallinity could be improved by introducing 1-chloronaphthalene (CN) additive in the perovskite precursor solution, which results in a 30% efficiency improvement compared with the reference devices.[25] Most recently, Wu et al. obtained high quality PbI_2 film with good coverage by

X. Gong, M. Li, X.-B. Shi, Dr. Z.-K. Wang, Prof. L.-S. Liao
Jiangsu Key Laboratory for Carbon-Based Functional Materials & Devices
Institute of Functional Nano & Soft Materials (FUNSOM)
Soochow University
Suzhou 215123, P. R. China
E-mail: zkwang@suda.edu.cn; lsliao@suda.edu.cn
X. Gong, Prof. H. Ma
College of Physics and Electronic Engineering
Henan Normal University
Xinxiang 453007, P. R. China

DOI: 10.1002/adfm.201503559

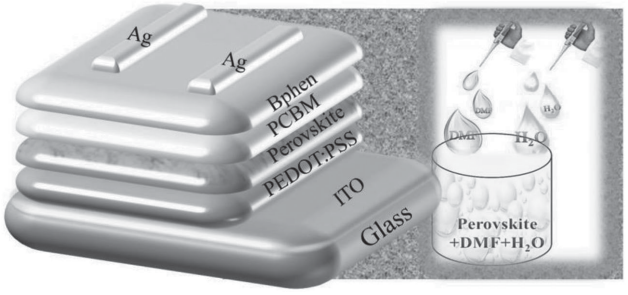

Figure 1. Device configuration of the planar perovskite solar cells and a schematic diagram of incorporating water additive into DMF-based perovskite precursor solutions.

adding a small amount of H_2O into PbI_2/*N*,*N*-dimethylformamide (DMF), which lead to a good efficiency of 18% in a two-step method based perovskite solar cell.[26] Conings et al. found that no precautions need to be taken concerning the anhydrous quality of the used precursor solvent when preparing the perovskite precursor solution after they investigated the impact of precursor water content on the performance of perovskite solar cells.[27]

In this work, we report a simple and effective method to control the growth of crystalline perovskite films by using water as a solvent additive for perovskite solution precursor. Incorporating of suitable amount of deionized water into the anhydrous DMF based perovskite precursor solutions can improve the crystallization of perovskite thin films with good film morphology and coverage. Accordingly, water additive based perovskite solar cells present a high PCE of 16.06% compared with the reference device (12.13%). More interestingly, the controlled devices demonstrate obviously improved ambient stability owing to the formation of stable perovskite hydrates by incorporating the water additive during the solution process.

2. Results and Discussion

We use a conventional planar heterojunction architecture of indium tin oxide (ITO)/PEDOT:PSS (40 nm)/$CH_3NH_3PbI_{3-x}Cl_x$ (300 nm)/$PC_{61}BM$ (50 nm)/Bphen (10 nm)/Ag (100 nm) (**Figure 1**) to study the influence of water additive on the crystalline perovskite films quality and the device stability. PEDOT:PSS interfacial layer is selected based on a consideration that it can ensure the better growth of high quality perovskite films, and

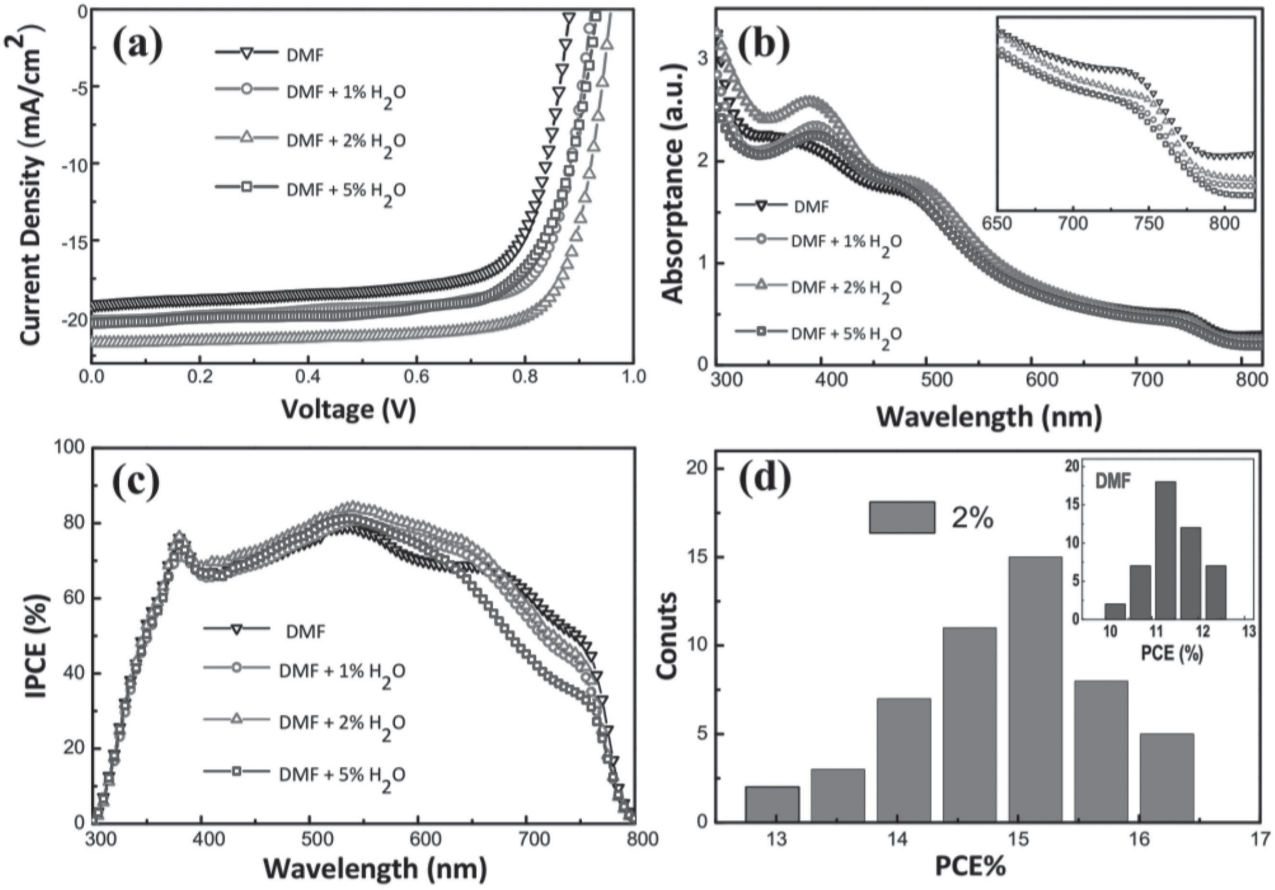

Figure 2. Performance and reproductivity of perovskite solar cells. a) *J*–*V* curves of devices with selected ratios of water additive in precursor solutions under AM 1.5G illumination of 100 mW cm^{-2}. b) Absorption spectra of corresponding devices. c) IPCE spectra of corresponding devices. d) A histogram of PCEs measured from 50 water additive (2%) based perovskite solar cells. Inset is the histogram of PCEs measured from 45 DMF-only-based perovskite solar cells.

Table 1. The cell performance of perovskite solar cells based on DMF solutions with and without water additive.

Solvent	J_{sc} [mA cm^{-2}]	$J_{sc\text{-}AVE}$ [mA cm^{-2}]	V_{oc} [V]	FF [%]	PCE [%]	PCE_{AVE} [%]	R_s [Ω]
DMF	19.12	18.98 ± 0.59	0.87	72.9	12.13	11.62 ± 0.40	77.26
DMF + 1% H_2O	20.21	19.63 ± 0.21	0.92	76.7	14.25	13.67 ± 0.62	40.48
DMF + 2% H_2O	21.67	20.78 ± 0.65	0.95	78.0	16.06	14.98 ± 0.54	33.12
DMF + 3% H_2O	21.39	20.39 ± 0.42	0.94	75.8	15.21	14.02 ± 0.62	38.22
DMF + 5% H_2O	20.51	19.84 ± 0.23	0.93	72.3	13.83	12.88 ± 0.41	47.38
DMF + 7% H_2O	19.58	19.36 ± 0.42	0.91	71.4	12.77	12.35 ± 0.25	57.40
DMF + 10% H_2O	18.93	17.53 ± 0.34	0.85	64.4	10.38	9.56 ± 0.38	98.34

provide sufficient charge dissociation and extraction.[6,17,28] Solution-processed Bphen is employed as an efficient cathode modification layer that can flatten the Ag cathode interface effectively.[29]

2.1. Perovskite Photovoltaic Performance

The deionized water was mixed with $CH_3NH_3PbI_{3-x}Cl_x$ blend in DMF with varied doping ratio from 2% to 10%. **Figure 2**a shows the current density–voltage (*J–V*) characteristics of $CH_3NH_3PbI_{3-x}Cl_x$ based perovskite solar cells with different doping ratio of deionized H_2O with DMF under AM 1.5 G conditions (100 mW cm^{-2}). The relevant performance parameters were summarized in **Table 1**. The reference device without any solvent additive exhibited a PCE of 12.13% with open circuit voltage (V_{oc}) of 0.87 V, short-circuit current density (J_{sc}) of 19.12 mA cm^{-2}, and fill factor (FF) of 72.9%. The cell performance was strongly dependent on the amount of deionized H_2O additive (Supporting Information, Figure S1 and Table S1). In the case of an optimized H_2O ratio of 2%, the device showed a significantly enhanced PCE of 16.06% with a V_{oc} of 0.95 V, J_{sc} of 21.67 mA cm^{-2} and FF of 78%. All cell parameters were improved via doping 2% H_2O in the perovskite precursor solution. By further increasing the amount of deionized H_2O, the cell parameters were decreased rapidly, especially in the case of higher doping ratio (10%) of deionized H_2O. Figure 2b presents the UV–vis absorption spectra of the perovskite films processed with different ratio of water additive. Apparently, perovskite film with 2% H_2O additive demonstrates the highest light absorption in the range of 300–600 nm. It should be noted that the absorption of H_2O additive based perovskite films decreases with the H_2O ratio obviously in the range of 600–800 nm (inset of Figure 2b), which is agreed well with the incident photon-to-current conversion efficiency (IPCE) measurement as shown in Figure 2c. We attributed it to a small change of the perovskite structure due to the water additive effect. Although the H_2O-additive based $CH_3NH_3PbI_{3-x}Cl_x$ perovskites belong to the same phase, the large difference of the crystal size and the film morphology may cause the changes of the parameters of perovskite unit cells, and therefore the variation of their absorption property. The details of water-assisted perovskite growth will be discussed later. For verifying the reproducibility of high efficiency of 2% water additive based PSCs, over 50 cells incorporating were fabricated. As shown by the histograms of PCE parameter in Figure 2d, the average power conversion efficiency reaches 13.69% with low relative standard deviation. In addition, the photocurrent hysteresis is found to be suppressed in 2% water additive based device based on a fact that the *J–V* curves were almost overlapped under forward and reverse bias scans or at different scanning rates (Supporting Information, Figure S2). The origin of the almost vanished photocurrent hysteresis will be given in the following section.

To clarify the nature of the influence of water additive, the morphology and coverage of perovskite films were evaluated. **Figure 3** shows the scanning electron microscopy (SEM) images of perovskite films incorporating with varied ratio of deionized H_2O. From Figure 3a, one can see that DMF-only-based perovskite films exhibit many small pin holes and voids. The existed defects and bad film coverage would lead to poor charge transport and weak light absorption in perovskite films. By introducing water additive, perovskite grain size is increased, and the voids on the perovskite film surface partly disappeared. In the case of 2% H_2O incorporating, almost continuous perovskite film with decreased grain boundaries can be observed as shown in Figure 3c. Notably, with further increase of the H_2O ratio, individual grain size is enlarged, whereas more and large voids are produced between the grains. The trend is more obvious in the case of 10% H_2O incorporating as shown in Figure 3g.

The X-ray diffraction spectrometry (XRD) patterns in **Figure 4** confirmed the role of water additive in the growth of perovskite crystal films. Strong diffraction peaks at 14.14° and 28.43° correspond to the diffractions from (110) and (220),[30] respectively, in crystal planes of $CH_3NH_3PbI_{3-x}Cl_x$ perovskite structure, which are consistent with the reported results.[15,16] $CH_3NH_3PbI_{3-x}Cl_x$ films present almost same XRD patterns which are independent on the H_2O additive ratio (Supporting Information, Figure S3). In addition, the inexistence of other impurity phases suggests a full conversion of the starting products to the perovskite phase in all samples. It means that there is no large influence of H_2O additive (below 10%) on the phase-purity of the $CH_3NH_3PbI_{3-x}Cl_x$ perovskites, which is consisted with the study reported by Conings et al.[27] Noticeably, 2% H_2O additive based $CH_3NH_3PbI_{3-x}Cl_x$ shows the strongest and sharpest diffraction peaks from (110), indicating the best crystallinity in this H_2O additive ratio.

Further investigation based on steady-state and time-resolved photoluminescence (PL) measurements were carried out to figure out the role of H_2O additive in the crystallization process

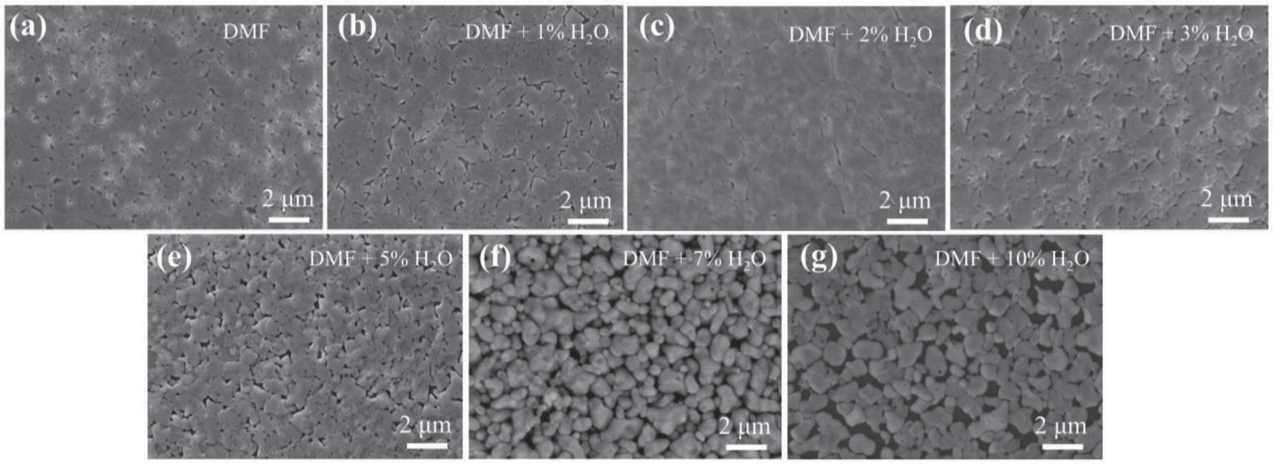

Figure 3. SEM images of $CH_3NH_3PbI_{3-x}Cl_x$ films based on a) DMF, b) DMF + 1% H_2O, c) DMF + 2% H_2O, d) DMF + 3% H_2O, e) DMF + 5% H_2O, f) DMF + 7% H_2O, and g) DMF + 10% H_2O solvent.

of the perovskites. As examples, the steady-state PL spectra of DMF and DMF+2% H_2O based perovskite films are shown in **Figure 5**a. The enhanced PL indicates that the nonradiative carrier recombination is significantly suppressed in 2% H_2O additive based perovskites. Furthermore, time-resolved PL spectra (Figure 5b) show that the 2% H_2O additive based perovskite films give an improved PL lifetime of ≈98 ns compared with the control perovskite film (36 ns). The results of steady-state and time-resolved PL measurements reveal that the nonradiative recombination channels in 2% H_2O additive based perovskite films could be inhibited to some extent. It suggests that the bulk defect in $CH_3NH_3PbI_{3-x}Cl_x$ perovskite films could be reduced by adding a small amount of water into the perovskite precursor. Heo et al. reported that enhanced crystallinity could be achieved by increasing the solubility of perovskite ionic compound in the solvent, since more concentrated solution would result in denser, smoother, and continuous crystalline films.[31] In present case, adding a small amount of water into DMF enhances the solubility of perovskite ionic compound, which is considered as one of main factors on the improved quality of the perovskite films. Noticeably, lower boiling point and higher vapor pressure of water (compared to DMF) would speed up the crystallization and result in the formation of large crystals as shown in Figure 3. Wu et al. reported that the hysteresis in photocurrent was more likely originated from the defects in the perovskite films, which can be suppressed by depositing a high quality perovskite film.[26] We assume that the suitable water additive could tune the perovskite crystallization with less defect, which inhibits the photocurrent hysteresis phenomenon. In addition, excess water addition (i.e., 10%) will lead to a poor morphology of the perovskite films, since water is only a good solvent for methylammonium iodide (MAI) but a bad solvent for $PbCl_2$.[32] The discontinuous morphology of the perovskite films with more and large voids would cause poor cell performance although larger crystal domains can be formed in higer H_2O additive ratio. The detailed role of water additive in tuning the perovskite crystallization is necessary to be investigated in the future by in situ techniques such as 2D grazing incidence XRD.

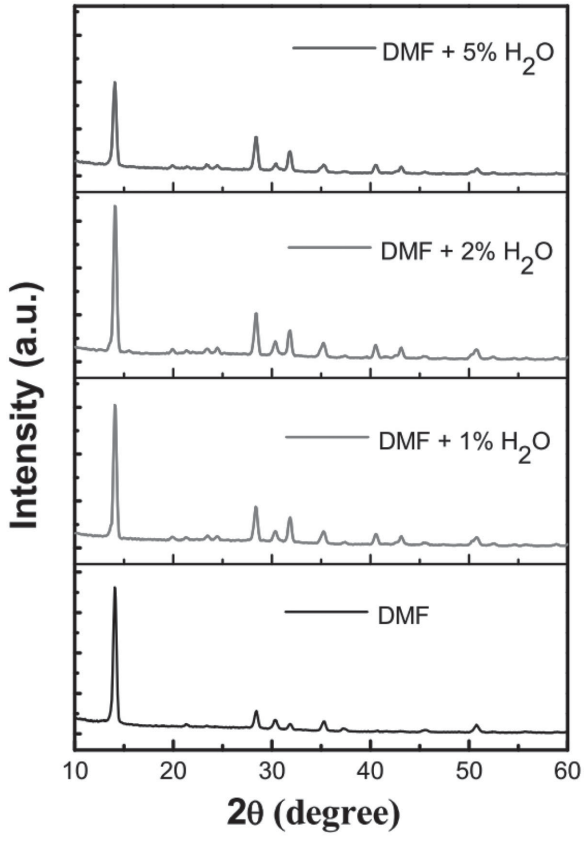

Figure 4. XRD patterns of $CH_3NH_3PbI_{3-x}Cl_x$ films based on a) DMF, b) DMF + 1% H_2O, c) DMF + 2% H_2O, and d) DMF + 5% H_2O solvent.

In all, incorporating water additive in DMF can control the oriented growth of perovskite crystal films with large grain size. By optimizing the doping ratio of H_2O additive, improved $CH_3NH_3PbI_{3-x}Cl_x$ films with large-scale domains and continuous film coverage can be obtained, which brings a combined effect of higher short-circuit current density, higher open-circuit

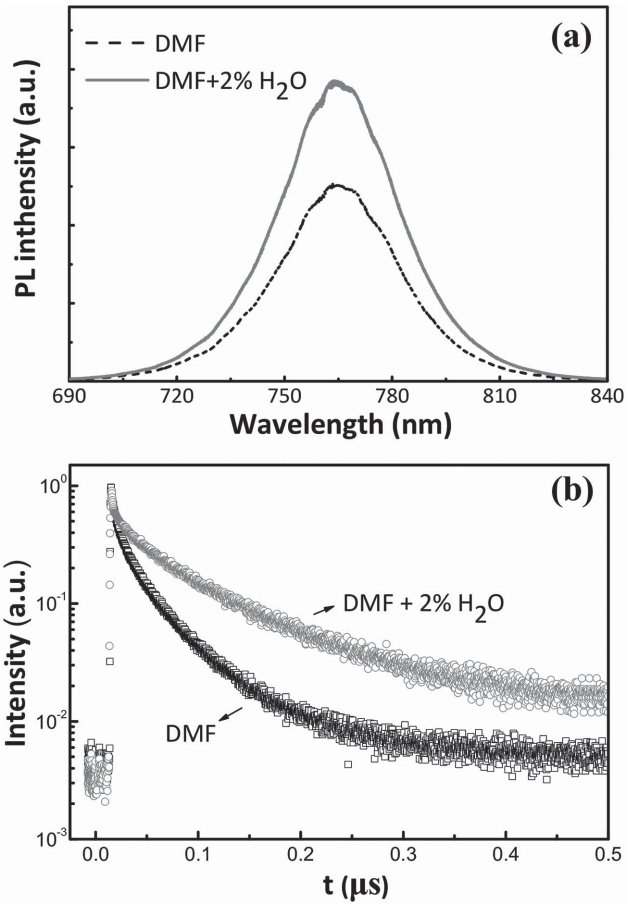

Figure 5. a) Steady-state and b) time-resolved PL measurements of perovskite film based on DMF and DMF + 2% H_2O solvent, the films are all coated on PEDOT:PSS surface.

voltage, and higher fill factor of the corresponding perovskite solar cells. We attributed it to the tunable evaporating rate of the mixed solvent and controllable nucleation time of the perovskite films by the water additive.[33,34]

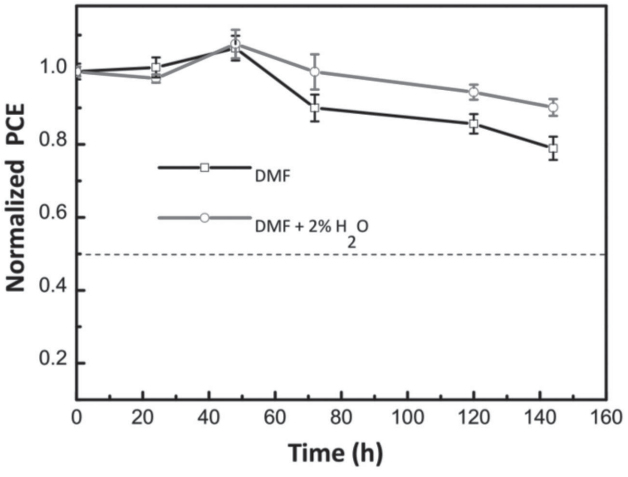

Figure 6. Cell stabilities of DMF and DMF + 2% H_2O based perovskite solar cells under ambient conditions.

2.2. Perovskite Photovoltaic Stability

From reported studies, organic–inorganic hybrid perovskite films easily degrade into other chemical species in the presence of moisture, and the degradation of the perovskite solar cells is ascribed to a reaction of perovskite film with water from the atmosphere.[21,35] The water would catalyze the decomposition of perovskite film.[36] Most probably, the perovskite solar cells in present work would present poor stability due to the incorporating of water additive. Unexpectedly, the water additive based devices exhibited better reliability than the DMF-only-based ones. For example, **Figure 6** shows the stability test of water additive (2%) and DMF-only-based perovskite solar cells without any encapsulation in ambient. In initial 50 h tests, the efficiency of both devices showed similar trend with continuous increasing till a maximum value. The phenomena of the efficiency rising till the maximum in primeval measurement is associated with a light soaking effect in perovskite solar cells.[37,38] The light illumination during measurement can reduce the density of charged bulk defects within the perovskite layer,[37] which leads to the efficiency rising to some extent. Afterward, water additive (2%) based device exhibited a good stability, the PCE only lowered to 92.8% of the maximum value after 150 h. For DMF-only-based device, the PCE first dropped to 87.5% of the maximum value rapidly, and then kept a stable trend. To clarify the origin of improved stablility in water additive (2%) based perovskite solar cells, SEM and XRD evaluations of the fresh and aged $CH_3NH_3PbI_{3-x}Cl_x$ films were carried out.

Figure 7 shows the SEM images of fresh and aged (150 h) $CH_3NH_3PbI_{3-x}Cl_x$ films with and without water additive (2%). Compared to the pristine films, many small white spots were

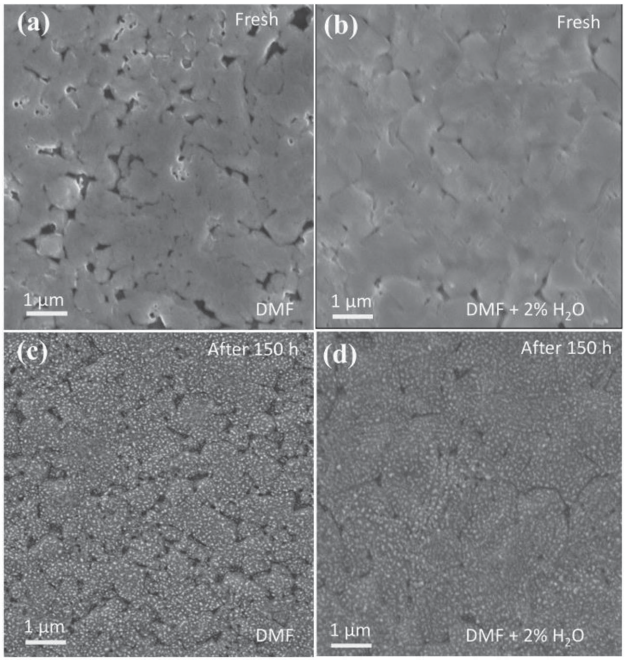

Figure 7. SEM images of fresh $CH_3NH_3PbI_{3-x}Cl_x$ films based on a) DMF and b) DMF + 2% H_2O, and aged (150 h) $CH_3NH_3PbI_{3-x}Cl_x$ films based on c) DMF and d) DMF + 2% H_2O.

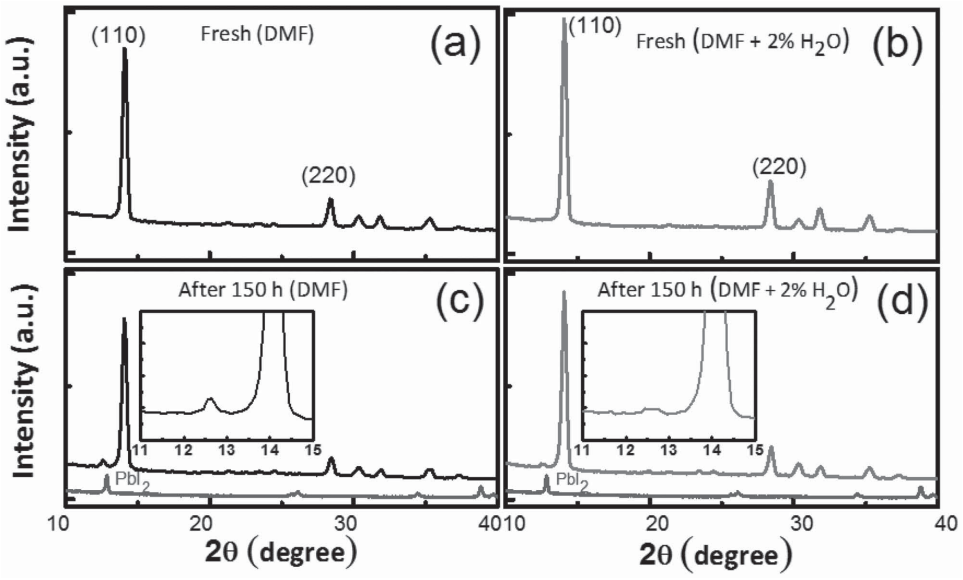

Figure 8. XRD patterns of fresh $CH_3NH_3PbI_{3-x}Cl_x$ films based on a) DMF, b) DMF + 2% H_2O, and aged (150 h) $CH_3NH_3PbI_{3-x}Cl_x$ films based on c) DMF, d) DMF + 2% H_2O.

distributed evenly throughout the surface of perovskite crystalline in the aged films, whereas the grain size of the aged pristine films was not changed. Relatively, the amount of the white spots in the water additive (2%) based aging films was less than the DMF-only based one obviously. The degradation of the perovskite layer exposing in the moist air may follow a decomposition pathway gradually. Similarly as the $CH_3NH_3PbI_3$, $CH_3NH_3PbI_{3-x}Cl_x$ ($x << 1$) first decomposes into CH_3NH_3I solution and PbI_2, then gradually decomposes into CH_3NH_2 solution and HI solution, finally HI also decomposes into I_2, H_2, H_2O in the light and oxygen environment.[38] To better understand the nature of the white spots and the degradation process of the perovskite solar cells, the evaluations of the cross section SEM images of the whole cells and the SEM/energy-dispersive X-ray (EDAX) in the fresh and aged samples were carried out (Supporting Information, Figure S4). Based on the content analysis of Pb, I, O, C, and N, the white spots appeared in the surface of the aged $CH_3NH_3PbI_{3-x}Cl_x$ were assumed to be the PbI_2.

To clarify this, XRD patterns of fresh and aged (150 h) $CH_3NH_3PbI_{3-x}Cl_x$ films with and without water additive (2%) were recorded as shown in **Figure 8**. Compared with the fresh samples, a signature peak at 12.65°, which is originated from the (001) diffraction peak of PbI_2 (Supporting Information, Figure S5), was observed in aged $CH_3NH_3PbI_{3-x}Cl_x$ films with and without water additive (2%). Meanwhile, the intensities of the (110) and (220) perovskite diffraction peaks were clearly reduced compared with the fresh samples. The appearance of (001) peak at 12.65° suggests that $CH_3NH_3PbI_{3-x}Cl_x$ films react with the water due to prolonged exposure in ambient, which results in the generation of PbI_2 since the decomposition of the $CH_3NH_3PbI_{3-x}Cl_x$ films. Notably, the intensity of (001) peak at 12.65° in water additive based perovskite film is obviously lower than that in DMF-only based perovskite film. It means that water additive based perovskite can resist the decomposition in moisture circumstance in some extent, which leads to improved cell stability as shown in Figure 6.

The behind nature of improved stability in the water additive based perovskite films can be ascribed as follows. We assumed that $CH_3NH_3PbI_{3-x}Cl_x \cdot nH_2O$ hydrates were generated during the annealing process, since the stabilization energies of the $CH_3NH_3PbI_{3-x}Cl_x \cdot nH_2O$ are lower than the total energy of the free $CH_3NH_3PbI_{3-x}Cl_x$ and nH_2O molecules. Therefore, $CH_3NH_3PbI_{3-x}Cl_x \cdot nH_2O$ based perovskite solar cells can be against the corrosion of water molecules in some extent owing to the stable $CH_3NH_3PbI_{3-x}Cl_x \cdot nH_2O$ system. Nevertheless, when $CH_3NH_3PbI_{3-x}Cl_x \cdot nH_2O$ system encounters more water molecules, the hydrogen bonds between the $PbI_{3-x}Cl_x$ and CH_3NH_3 units will be destroyed, which induces a decomposition of $CH_3NH_3PbI_{3-x}Cl_x$ and then deteriorate the cell stability.[39,40] Presently, a complete confirmation of the $CH_3NH_3PbI_{3-x}Cl_x \cdot nH_2O$ generation and the number of H_2O molecules in $CH_3NH_3PbI_{3-x}Cl_x \cdot nH_2O$ system is difficult since the conditionality of the crystal perovskite films preparation and the matching of the evaluating techniques. However, a qualitative evaluation based on element analysis using EDAX (Supporting Information, Figure S6) and weight measurement using thermogravimetric analysis (TGA) can give some informaton on the formation of the $CH_3NH_3PbI_{3-x}Cl_x \cdot nH_2O$ hydrates (Supporting Information, Figure S7). The EDAX analysis indicated that the 2% H_2O additive based perovskite sample contains 2.39 wt% oxygen element (in contrast zero oxygen content in the control perovskite sample). The TGA measurement demonstrated that there was a very obvious weight loss when the sample was heated to 253 °C, whereas no large weight variation was observed in the control sample. Both of the experiments suggest a possibility that the H_2O molecules existed in the $CH_3NH_3PbI_{3-x}Cl_x$ perovskites. Further experiment evidences are necessary in the future by using advanced techniques and subtle experiment design.

3. Conclusions

In summary, we have investigated the influence of water additives on perovskite thin films and the corresponding device performance. 2% water additive can enhance the crystallization, the surface coverage, and the stability of perovskite thin films effectively, which results in significant enhancement of PCE from 12.13% to 16.06% and cell stability under ambient conditions. Incorporating suitable water additive in DMF can control the oriented growth of perovskite crystal films. By tracing the change of morphology and electrical structure of perovskite films with time in air, $CH_3NH_3PbI_{3-x}Cl_x \cdot nH_2O$ hydrated perovskites were assumed to be generated during the annealing process, which can be resistant to the corrosion by water molecules to some extent. The findings in this work provide a new route to control the growth of crystal perovskites and a clue to improve the stability of organic–inorganic halide perovskites.

4. Experimental Section

Preparation of $CH_3NH_3PbI_{3-x}Cl_x$ Perovskite Solution: MAI was synthesized by reacting 20 mL of hydroiodic acid (57 wt% in H_2O) and 48 mL methylamine (40 wt% in methanol) in a 250 mL round-bottom flask under ice bath for 2 h with stirring. The reactants products were distilled in the rotary evaporator at 55 °C to remove the solvents and then the precipitate was washed by diethyl ether three times. Finally, white-colored powder was collected and dried at 60 °C for 24 h in vacuum. To prepare the perovskite precursor solution, MAI and lead chloride ($PbCl_2$, 99.999%) powder were mixed in anhydrous DMF (99.9%) with a molar ratio of 3:1. The perovskite/water solution was prepared via adding different volume ratio of deioned water into the perovskite precursor solution. The mixture solutions were stirred at 60 °C overnight in a glovebox and filtered with a 0.45 μm Polytetrafluoroethylene (PTFE) filter before device fabrication.

Device Fabrication: The ITO-coated glass substrates (≈15 Ω sq^{-1}) were first cleaned with detergent, then ultrasonicated in acetone and ethanol at room temperature for 12 min, and subsequently treated in UV–ozone cleaner for 15 min. A film (≈40 nm) of PEDOT:PSS (Baytron PVP Al 4083) was spin-coated onto the ITO substrate at 4500 rpm for 40 s and then annealed at 140 °C for 10 min. The substrates were transferred into a glovebox to thin-film perovskite layers coating. A 30 wt% $CH_3NH_3PbI_{3-x}Cl_x$ precursor solution with and without water was spin-coated at 4000 rpm for 40 s. After the perovskite films were dried at room temperature for 20 min, the samples were annealed on a hot plate by a typical gradient increased temperature method. Afterward, the $PC_{61}BM$ (20 mg mL^{-1} in chloroform) and Bphen (0.5 mg mL^{-1} in absolute ethanol) were then sequentially deposited by spin coating at 2000 rpm for 40 s and 4000 rpm for 40s, respectively. Finally, the samples were transferred to a vacuum chamber and then 100 nm Ag (mask area of 7.25 mm^2) was deposited on top of the Bphen layer by thermal evaporation under 10^{-7} Torr.

Device Characterization: The surface morphologies of $CH_3NH_3PbI_{3-x}Cl_x$ films with different water doped were characterized using a field-emission SEM (Quanta 200 FEG, FEI Co.) XRD pattern was measured using a PANalytical 80 equipment (Empyrean, Cu Ka radiation). The absorption spectra of the substrates were conducted on an UV/vis spectrophotometer (PerkinElmer Lambda 750). The photocurrent density–voltage (*J–V*) characteristics of PSCs were recorded under 1 sun illumination using a programmable Keithley 2400 source meter under AM 1.5G simulated solar light. The steady state PL spectra and timer time-resolved PL were obtained by Horiba Jobin-Yvon LabRAM HR800 and a single photon counting spectrometer which was combined with the Fluorolog-3 spectrofluorometer (Horiba-FM-2015). A 625 nm laser source was used in the time resolved PL measurement. IPCE measurements were measured by a Newport monochromator 74125 and power meter 1918 with silicon detector 918D measurement system. The TGA was carried out by utilizing thermogravimetric analyzer (FR-TGA-10). Automatic control procedures of four successive phases are: heating up (25–300 °C)—temperature stabilizing (300 °C)—cooling down (300–25 °C)—stop machine. Each phase's time is 30 min, rates of heating and cooling are 10 °C min^{-1}.

Supporting Information

Supporting Information is available from the Wiley Online Library or from the author.

Acknowledgements

X.G. and M.L. contributed equally to this work. The authors acknowledge financial support from the Natural Science Foundation of China (Grant nos. 61307036 and 61177016) and from the Natural Science Foundation of Jiangsu Province (Grant no. BK20130288). This project was also funded by the Collaborative Innovation Center of Suzhou Nano Science and Technology, and by the Priority Academic Program Development of Jiangsu Higher Education Institutions (PAPD).

Received: August 23, 2015
Published online: October 1, 2015

[1] a) J.-W. Cheng, S.-T. Zheng, G.-Y. Yang, *Inorg. Chem.* **2007**, *46*, 10261; b) S. Kazim, M. K. Nazeeruddin, M. Grätzel, S. Ahmad, *Angew. Chem. Int. Ed.* **2014**, *53*, 2812; c) K. Wojciechowski, S. D. Stranks, A. Abate, G. Sadoughi, A. Sadhanala, N. Kopidakis, G. Rumbles, C.-Z. Li, R. H. Friend, A. K.-Y. Jen, *ACS Nano* **2014**, *8*, 12701.

[2] J. M. Ball, M. M. Lee, A. Hey, H. J. Snaith, *Energy Environ. Sci.* **2013**, *6*, 1739.

[3] C. W. Chen, H. W. Kang, S. Y. Hsiao, P. F. Yang, K. M. Chiang, H. W. Lin, *Adv. Mater.* **2014**, *26*, 6647.

[4] G. Xing, N. Mathews, S. Sun, S. S. Lim, Y. M. Lam, M. Grätzel, S. Mhaisalkar, T. C. Sum, *Science* **2013**, *342*, 344.

[5] M. Liu, M. B. Johnston, H. J. Snaith, *Nature* **2013**, *501*, 395.

[6] S. D. Stranks, G. E. Eperon, G. Grancini, C. Menelaou, M. J. Alcocer, T. Leijtens, L. M. Herz, A. Petrozza, H. J. Snaith, *Science* **2013**, *342*, 341.

[7] C. Wehrenfennig, G. E. Eperon, M. B. Johnston, H. J. Snaith, L. M. Herz, *Adv. Mater.* **2014**, *26*, 1584.

[8] H. Zhou, Q. Chen, G. Li, S. Luo, T.-B. Song, H.-S. Duan, Z. Hong, J. You, Y. Liu, Y. Yang, *Science* **2014**, *345*, 542.

[9] a) W. Nie, H. Tsai, R. Asadpour, J.-C. Blancon, A. J. Neukirch, G. Gupta, J. J. Crochet, M. Chhowalla, S. Tretiak, M. A. Alam, *Science* **2015**, *347*, 522; b) N. J. Jeon, J. H. Noh, W. S. Yang, Y. C. Kim, S. Ryu, J. Seo, S. I. Seok, *Nature* **2015**, *517*, 476; c) Q. Chen, H. Zhou, Z. Hong, S. Luo, H.-S. Duan, H.-H. Wang, Y. Liu, G. Li, Y. Yang, *J. Am. Chem. Soc.* **2013**, *136*, 622.

[10] A. Kojima, K. Teshima, Y. Shirai, T. Miyasaka, *J. Am. Chem. Soc.* **2009**, *131*, 6050.

[11] a) H. J. Snaith, *J. Phys. Chem. Lett.* **2013**, *4*, 3623; b) H.-S. Kim, C.-R. Lee, J.-H. Im, K.-B. Lee, T. Moehl, A. Marchioro, S.-J. Moon, R. Humphry-Baker, J.-H. Yum, J. E. Moser, *Sci. Rep.* **2012**, *2*. 591; c) M. M. Lee, J. Teuscher, T. Miyasaka, T. N. Murakami, H. J. Snaith, *Science* **2012**, *338*, 643; d) A. Abate, D. J. Hollman, J. L. Teuscher,

S. Pathak, R. Avolio, G. D'Errico, G. Vitiello, S. Fantacci, H. J. Snaith, *J. Am. Chem. Soc.* **2013**, *135*, 13538.
[12] J. Burschka, N. Pellet, S.-J. Moon, R. Humphry-Baker, P. Gao, M. K. Nazeeruddin, M. Grätzel, *Nature* **2013**, *499*, 316.
[13] M. Xiao, F. Huang, W. Huang, Y. Dkhissi, Y. Zhu, J. Etheridge, A. Gray-Weale, U. Bach, Y. B. Cheng, L. Spiccia, *Angew. Chem.* **2014**, *126*, 10056.
[14] C.-C. Chueh, C.-Y. Liao, F. Zuo, S. T. Williams, P.-W. Liang, A. K.-Y. Jen, *J. Mater. Chem. A.* **2015**, *3*, 9058.
[15] C.-Y. Chang, C.-Y. Chu, Y.-C. Huang, C.-W. Huang, S.-Y. Chang, C.-A. Chen, C.-Y. Chao, W.-F. Su, *ACS Appl. Mater. Interfaces* **2015**, *7*, 4955.
[16] Z.-K. Wang, M. Li, D.-X. Yuan, X.-B. Shi, H. Ma, L.-S. Liao, *ACS Appl. Mater. Interfaces.* **2015**, *7*, 9645.
[17] M. Qian, M. Li, X. Shi, H. Ma, Z.-K. Wang, L. Liao, *J. Mater. Chem. A* **2015**, *3*, 13533.
[18] a) T. Baikie, Y. Fang, J. M. Kadro, M. Schreyer, F. Wei, S. G. Mhaisalkar, M. Graetzel, T. J. White, *J. Mater. Chem. A* **2013**, *1*, 5628; b) H. J. Snaith, M. Grätzel, *Adv. Mater.* **2006**, *18*, 1910.
[19] a) T. Leijtens, G. E. Eperon, S. Pathak, A. Abate, M. M. Lee, H. J. Snaith, *Nat. Commun.* **2013**, *4*, 2885; b) J. H. Noh, S. H. Im, J. H. Heo, T. N. Mandal, S. I. Seok, *Nano Lett.* **2013**, *13*, 1764; c) B. J. Kim, D. H. Kim, Y.-Y. Lee, H.-W. Shin, G. S. Han, J. S. Hong, K. Mahmood, T. K. Ahn, Y.-C. Joo, K. S. Hong, *Energy Environ. Sci.* **2015**, *8*, 916; d) S. N. Habisreutinger, T. Leijtens, G. E. Eperon, S. D. Stranks, R. J. Nicholas, H. J. Snaith, *Nano Lett.* **2014**, *14*, 5561.
[20] J. You, Y. M. Yang, Z. Hong, T.-B. Song, L. Meng, Y. Liu, C. Jiang, H. Zhou, W.-H. Chang, G. Li, *Appl. Phys. Lett.* **2014**, *105*, 183902.
[21] K. K. Bass, R. E. McAnally, S. Zhou, P. I. Djurovich, M. E. Thompson, B. C. Melot, *Chem. Commun.* **2014**, *50*, 15819.
[22] Z. Yang, C. C. Chueh, F. Zuo, J. H. Kim, P. W. Liang, A. K. Y. Jen, *Adv. Energy. Mater.* **2015**, *5*, 1.
[23] a) J. Y. Jeng, Y. F. Chiang, M. H. Lee, S. R. Peng, T. F. Guo, P. Chen, T. C. Wen, *Adv. Mater.* **2013**, *25*, 3727; b) G. E. Eperon, V. M. Burlakov, P. Docampo, A. Goriely, H. J. Snaith, *Adv. Funct. Mater.* **2013**, *24*, 15.
[24] P. W. Liang, C. C. Chueh, X. K. Xin, F. Zuo, S. T. Williams, C. Y. Liao, A. K. Y. Jen, *Adv. Energy Mater.* **2015**, *5*, 1400960.
[25] X. Song, W. Wang, P. Sun, W. Ma, Z.-K. Chen, *Appl. Phys. Lett.* **2015**, *106*, 033901.
[26] C. G. Wu, C. H. Chiang, Z. L. Tseng, M. K. Nazeeruddin, A. Hagfeldt, M. Grätzel, *Energy Environ. Sci.* **2015**, *8*, 2725.
[27] B. Conings, A. Babayigit, T. Vangerven, J. D'Haen, J. Manca, H. G. Boyen, *J. Mater. Chem. A* **2015**, *3*, 19123.
[28] a) D.-X. Yuan, A. Gorka, M.-F. Xu, Z.-K. Wang, L. Liao, *Phys. Chem. Chem. Phys.* **2015**, *17*, 19745; b) P. Docampo, J. M. Ball, M. Darwich, G. E. Eperon, H. J. Sniath, *Nat. Commun.* **2013**, *4*, 2761.
[29] M.-F. Xu, L.-S. Cui, X.-Z. Zhu, C.-H. Gao, X.-B. Shi, Z.-M. Jin, Z.-K. Wang, L.-S. Liao, *Org. Electron.* **2013**, *14*, 657.
[30] B. Conings, L. Baeten, C. De Dobbelaere, J. D'Haen, J. Manca, H. G. Boyen, *Adv. Mater.* **2014**, *26*, 2041.
[31] J. H. Heo, D. H. Song, S. H. Im, *Adv. Mater.* **2014**, *26*, 8179.
[32] H. L. Clever, F. J. Johnston, *J. Phys. Chem. Ref. Data* **1980**, *9*, 751.
[33] P. Stephens, F. Devlin, C. Chabalowski, M. J. Frisch, *J. Phys. Chem.* **1994**, *98*, 11623.
[34] P. W. Liang, C. Y. Liao, C. C. Chueh, F. Zuo, S. T. Williams, X. K. Xin, J. Lin, A. K. Y. Jen, *Adv. Mater.* **2014**, *26*, 3748.
[35] a) J. Cao, J. Yin, S. Yuan, Y. Zhao, J. Li, N. Zheng, *Nanoscale* **2015**, *7*, 9443; b) G. Sfyri, C. V. Kumar, D. Raptis, V. Dracopoulos, P. Lianos, *Sol. Energy Mater. Sol. Cells* **2015**, *134*, 60; c) A. Fakharuddin, F. Di Giacomo, I. Ahmed, Q. Wali, T. M. Brown, R. Jose, *J. Power Sources* **2015**, *283*, 61.
[36] J. M. Frost, K. T. Butler, F. Brivio, C. H. Hendon, M. Van Schilfgaarde, A. Walsh, *Nano Lett.* **2014**, *14*, 2584.
[37] C. Zhao, B. Chen, X. Qiao, L. Luan, K. Lu, B. Hu, *Adv. Energy Mater.* **2015**, DOI:10.1002/aenm.201570076.
[38] S. Lv, S. Pang, Y. Zhou, N. P. Padture, H. Hu, L. Wang, G. Cui, *Phys. Chem. Chem. Phys.* **2014**, *16*, 19206.
[39] X. Dong, X. Fang, M. Lv, B. Lin, S. Zhang, J. Ding, N. Yuan, *J. Mater. Chem. A* **2015**, *3*, 5360.
[40] J. A. Christians, P. A. Miranda Herrera, P. V. Kamat, *J. Am. Chem. Soc.* **2015**, *137*, 1530.